Measurement Science and Technology

100 year anniversary
Measurement Science and Technology

TOPICAL REVIEW

Multi-spectral pyrometry—a review

To cite this article: António Araújo 2017 *Meas. Sci. Technol.* **28** 082002

IOP Publishing Measurement Science and Technology
Meas. Sci. Technol. **28** (2017) 082002 (15pp) https://doi.org/10.1088/1361-6501/aa7b4b

Topical Review

Multi-spectral pyrometry—a review

António Araújo

Faculdade de Engenharias e Tecnologias, Universidade Lusíada Norte, 4760-108 Vila Nova de Famalicão, Portugal

E-mail: antonio.araujo@hotmail.com

Received 1 June 2017, revised 15 June 2017
Accepted for publication 23 June 2017
Published 17 July 2017

Abstract

In pyrometry measurements, the unknown target emissivity is a critical source of uncertainty, especially when the emissivity is low. Aiming to overcome this problem, various multi-spectral pyrometry systems and processing techniques have been proposed in the literature. Basically, all multi-spectral systems are based on the same principle: the radiation emitted by the target is measured at different channels having different spectral characteristics, and the emissivity is modelled as a function of wavelength with adjustable parameters to be obtained empirically, resulting in a system of equations whose solution is the target temperature and the parameters of the emissivity function. The present work reviews the most important multi-spectral developments. Concerning the spectral width of the measurement channels, multi-spectral systems are divided into multi-wavelength (monochromatic channels) and multi-band (wide-band channels) systems. Regarding the number of unknowns and equations (one equation per channel), pyrometry systems can either be determined (same number of unknowns and equations, having a unique solution) or overdetermined (more equations than unknowns, to be solved by least-squares). Generally, higher-order multi-spectral systems are overdetermined, since the uncertainty of the solutions obtained from determined systems increases as the number of channels increases, so that determined systems normally have less than four channels. In terms of the spectral characteristics of the measurement channels, narrow bands, far apart from each other and shifted towards lower wavelengths, seem to provide more accurate solutions. Many processing techniques have been proposed, but they strongly rely on the relationship between emissivity and wavelength, which is, in turn, strongly dependent on the characteristics of a particular target. Several accurate temperature and/or emissivity results have been reported, but no universally accepted multi-spectral technique has yet been developed.

Keywords: temperature, emissivity, pyrometry, multi-wavelength, multi-band

(Some figures may appear in colour only in the online journal)

1. Introduction

For absolute temperature T, per unit area and unit solid angle, maximum thermal radiation power is emitted by an ideal black surface (black body) according to Planck's spectral distribution [1, 2]:

$$L_b(\lambda, T) = \frac{c_1}{\lambda^5 \left(\exp \frac{c_2}{\lambda T} - 1\right)}, \quad (1)$$

where λ is the wavelength, and $c_1 = 1.1910 \times 10^8$ W μm^4 m^{-2} sr^{-1} and $c_2 = 1.4388 \times 10^4$ μm K are the first and second radiation constants, respectively. Wien's spectral distribution is a simplified approximation of Planck's distribution, valid when $\lambda T \ll c_2$ (short wavelengths and low temperatures) [1, 2], in which

$$L_b(\lambda, T) = \frac{c_1}{\lambda^5 \exp \frac{c_2}{\lambda T}}. \quad (2)$$

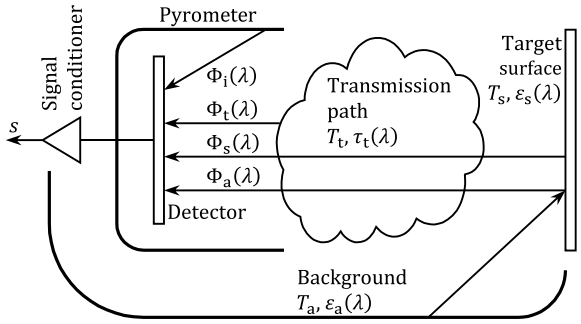

Figure 1. Pyrometry radiation fluxes.

However, only a fraction of black-body radiation is emitted by a real surface:

$$L(\lambda, T) = \varepsilon(\lambda) L_b(\lambda, T), \tag{3}$$

where $0 \leqslant \varepsilon(\lambda) \leqslant 1$ is the spectral emissivity, which is a function of λ (the variation of emissivity with emitting direction and temperature is omitted for simplicity). A special type of surface is the so-called grey surface (grey body), in which $\varepsilon(\lambda)$ does not change with varying λ.

A pyrometer is a non-contact device that intercepts and absorbs thermal radiation from an emitting target surface, consisting of an optical system that focuses the incoming radiation onto a detector [3]. Most surfaces encountered in engineering applications emit thermal radiation in the infrared (IR) range, so that most detectors operate in this range, being generally termed IR detectors [4]. The output signal of a detector is related to the temperature of the target surface according to a transfer function, normally obtained by calibration with a black body. In real surfaces, as $\varepsilon(\lambda) < 1$, the emitted radiation will be different from that of a black body at the same temperature, so that the pyrometer will consequently provide a different temperature reading from that of the target surface; therefore, the emissivity of the emitting surface must be determined, so as to correct the temperature output of the pyrometer to the true temperature of the target surface.

As shown in figure 1, at wavelength λ, four main spectral radiation fluxes reach the detector of a pyrometer [5]: radiation emitted by the target surface ($\Phi_s(\lambda)$); radiation emitted by the background surfaces and reflected by the target surface ($\Phi_a(\lambda)$); radiation emitted by the transmission path ($\Phi_t(\lambda)$); radiation emitted by the inner surfaces of the pyrometer ($\Phi_i(\lambda)$).

The spectral radiation emitted by the target surface and reaching the detector

$$\Phi_s(\lambda) = \varepsilon_s(\lambda)\tau_t(\lambda) L_b(\lambda, T_s), \tag{4}$$

where $\varepsilon_s(\lambda)$ is the spectral emissivity of the target surface, $\tau_t(\lambda)$ is the spectral transmissivity of the transmission path between the target surface and the detector, and T_s is the temperature of the target surface.

In most practical cases, the medium of the the transmission path is atmospheric air, whose transmissivity is dependent on wavelength and distance, so that IR devices normally operate in bands of maximum transmissivity, such as the so-called short-wave range (2–5 μm) and the long-wave range (8–14 μm) [3, 5]. In the long-wave range and sections of the short-wave range, for relatively short distances, equation (4) can be simplified, since atmospheric attenuation can be ignored, i.e. $\tau_t(\lambda) \approx 1$ [2].

So as to simplify, it can be assumed that all background surfaces are at a single temperature T_a, acting as a black body relative to the target surface, i.e. $\varepsilon_a(\lambda) \approx 1$, since the background surfaces completely surround the target surface [6]. Therefore, the spectral radiation emitted by the background surfaces, reflected by the target surface, and reaching the detector

$$\Phi_a(\lambda) = [1 - \varepsilon_s(\lambda)]\tau_t(\lambda) L_b(\lambda, T_a), \tag{5}$$

where, according to Kirchhoff' s law and the balance of the radiation fluxes on the target surface, the spectral reflectivity of the target surface $\rho_s(\lambda) = 1 - \varepsilon_s(\lambda)$ [1–3]. In the derivation of equation (5), the attenuation effects between the background surfaces and the target surface were omitted for simplicity. Similarly to equation (4), for short distances and spectral ranges of high transmissivity, equation (5) can be simplified as $\tau_t(\lambda) \approx 1$.

The spectral radiation emitted by the transmission path and reaching the detector

$$\Phi_t(\lambda) = [1 - \tau_t(\lambda)] L_b(\lambda, T_t), \tag{6}$$

where T_t is the temperature of the medium of the transmission path. The emissivity of the transmission path $\varepsilon_t(\lambda) = 1 - \tau_t(\lambda)$, and if, as assumed before, $\tau_t(\lambda) \approx 1$, then $\Phi_t(\lambda)$ can be ignored [2].

Minkina *et al* [5] indicated that the influence of internal radiation $\Phi_i(\lambda)$ on radiation measurements can be disregarded. Araújo and co-workers [7–10] also showed that if $\Phi_i(\lambda)$ does not vary significantly between measurements, its effect can neglected.

Generally, the output signal (s) of a pyrometer is proportional to the spectral integration of the four aforementioned radiation fluxes [5], absorbed by the detector according to its spectral response ($\alpha_d(\lambda)$), which includes the spectral absorptivity of the detector, and it may also include other effects, such as prior attenuation of the incoming radiation caused, for example, by the optical system. If atmospheric attenuation is neglected,

$$s = k \int_{\lambda=\lambda'}^{\lambda''} \alpha_d(\lambda) \{\varepsilon_s(\lambda) L_b(\lambda, T_s) + [1 - \varepsilon_s(\lambda)] L_b(\lambda, T_a) + \Phi_i(\lambda)\} \, d\lambda, \tag{7}$$

where λ' and λ'' are the lower and upper cut-off wavelengths, respectively, and k is a proportionality constant, which depends mainly on the gain of the electronic system.

The calibration of pyrometers is generally performed with a black body, in which $\varepsilon_s(\lambda) = 1$ at different temperatures $T_s = T$, so that equation (7) can be simplified to give the output signal of the radiation measurement of a black body:

$$s_b = k \int_{\lambda=\lambda'}^{\lambda''} \alpha_d(\lambda) [L_b(\lambda, T) + \Phi_i(\lambda)] \, d\lambda. \tag{8}$$

By equating s (7) to s_b (8), and by assuming that $\Phi_i(\lambda)$ does not vary significantly between measurements, the following equation can be derived:

$$\int_{\lambda=\lambda'}^{\lambda''} \alpha_d(\lambda)\{\varepsilon_s(\lambda)L_b(\lambda,T_s)+[1-\varepsilon_s(\lambda)]L_b(\lambda,T_a)\}\,d\lambda = \int_{\lambda=\lambda'}^{\lambda''} \alpha_d(\lambda)L_b(\lambda,T)\,d\lambda. \quad (9)$$

The implicit solution of temperature T from equation (9) represents the effective radiance temperature, i.e. the pyrometer temperature output from the measurement of a target surface at temperature T_s and spectral emissivity $\varepsilon_s(\lambda)$, when the background surfaces are at temperature T_a.

In practice, the calibration of pyrometers with a black body is often modelled with semi-empirical adaptations of equation (8), such as the Sakuma–Hattori equation [11–14], which is based on Wien's distribution; a Planck's distribution version of the Sakuma–Hattori equation has also been formulated [13–15]:

$$s_b = \frac{K}{\exp\left(\frac{c_2}{AT+B}\right)-1}, \quad (10)$$

where A, B, and K are parameters to be obtained experimentally by data fitting with data from the calibration procedure. Other calibration relationships, such as polynomial functions, have also been used [5, 14, 16–19].

Generally, in multi-spectral pyrometry, $n \geqslant 2$ spectral channels simultaneously measure the radiation emitted by a target surface with unknown emissivity, where each spectral channel corresponds to a different spectral content. The basic principle of any multi-spectral pyrometer is that the emissivity is modelled as a smooth function of wavelength, containing $m \leqslant n-1$ unknown parameters, resulting in a system of n equations with $m+1$ unknowns (emissivity parameters and surface temperature). In determined systems, $n = m+1$, so that there is a unique solution for temperature and emissivity function parameters [20]; in overdetermined systems, $n > m+1$, and an optimal solution for temperature and emissivity parameters can be computed by least-squares [21]. However, up until recently, unlike dual-spectral systems, multi-spectral pyrometry systems were not so widely applied into industrial applications [22]. Pyrometry systems with very narrow spectral bands, in which the incoming radiation can be assumed to be absorbed at a single wavelength (monochromatic radiation), are named multi-wavelength pyrometers; pyrometry systems with spectral bands of finite width are named multi-band pyrometers.

Practical implementations of multi-spectral pyrometry include the measurement of surface temperature and/or emissivity of different processes and applications, such as wire drawing [23], welding operations [24–28], heat treatment processes [29, 30], metal removal processes [18, 31–35], laser melting processes [36, 37], braking temperature monitoring [38–40], temperature monitoring of gas turbine blades [41–45], and seawater surface temperature measurements [46]. Another important application is the analysis of combustion processes in diesel engines through the measurement of the temperature and/or concentration of soot [47–53].

The objective of the current paper is to present a review on multi-spectral pyrometry and its most relevant advances. The following section is dedicated to dual-wavelength pyrometry; this section is further divided into surface pyrometry and soot pyrometry of combustion flames. Afterwards, determined and overdetermined multi-wavelength systems are comparatively evaluated in terms of their advantages, limitations, and modelling techniques. The last section is dedicated to dual-band and higher-order multi-band pyrometry systems. Only naturally-emitted radiation methods are addressed; indirect methods based on radiation generated by an external source and reflected by the target surface are outside the scope of the present work.

2. Dual-wavelength pyrometry

Dual-wavelength or dual-colour pyrometers are multi-wavelength systems, in which $n = 2$ radiation measurements are performed at two different monochromatic wavelengths. There are two main applications for dual-wavelength pyrometers: surface pyrometry, in which the measurements are performed to a surface of unknown emissivity, or when only part of the target surface is in field-of-view of the measurements; soot pyrometry, in which the measurements are performed with the radiation emitted by the soot particles present in the flame of combustion processes.

2.1. Surface pyrometry

In surface pyrometry, simplest dual-wavelength systems are based on the following assumptions: the background is cool enough relative to the target surface, so that background radiation effects can be neglect, i.e. $\Phi_a(\lambda) \approx 0$ W μm^{-1} m^{-2} sr^{-1} [2, 54] (reflected radiation can be a serious problem when the temperature of the target surface is not much different from that of its surroundings, and, in this case, single-wavelength pyrometry becomes a better option, since the target surface acts as a black body when it is at the same temperature as the background [7, 8, 10, 55]); the emission of black-body spectral radiation is modelled by Wien's distribution (2); the spectral bands are so narrow, i.e. $\lambda' \approx \lambda''$, that all incoming radiation is assumed to be absorbed at a discrete wavelength λ, avoiding the wavelength integration of Wien's distribution [56]. There are two modelling approaches to dual-wavelength pyrometry: the radiation method, in which the outputs of the spectral measurements are proportional to the incoming radiation [54]; the temperature method, in which the outputs of the spectral measurements are proportional to the inferred temperatures [57].

Tenney [54] indicated that dual-wavelength pyrometers do not necessary provide more accurate results than single-wavelength pyrometers and identified three typical application areas of dual-wavelength pyrometry: grey bodies with unknown emissivity; partial targets, in which the target surface does not completely fill the field-of-view of the pyrometer;

obstructed targets, in which the target surface is obstructed by an extraneous body.

2.1.1. Radiation method. In the radiation method, equation (7) is simplified according to the aforementioned assumptions, and internal radiation $\Phi_i(\lambda)$ is neglected, resulting in the following system of two equations for the two spectral channels $i = 1$ and 2:

$$s_i = k_i \varepsilon_{s,i} L_b(\lambda_i, T_s), \tag{11}$$

where s_i is the output signal, k_i is a proportionality constant, obtainable from the calibration process, that depends on the electronic gain, system optics, and detector response at wavelength λ_i, and $\varepsilon_{s,i} = \varepsilon_s(\lambda_i)$ is the emissivity of the target surface at wavelength λ_i. Solving equation (11) for T_s results in the so-called radiation ratio equation [54]:

$$\frac{1}{T_s} = \frac{\lambda_1 \lambda_2}{c_2(\lambda_2 - \lambda_1)} \left(\ln \frac{s_2 k_1}{s_1 k_2} + 5 \ln \frac{\lambda_2}{\lambda_1} + \ln \frac{\varepsilon_{s,1}}{\varepsilon_{s,2}} \right). \tag{12}$$

For a grey surface (although many surfaces do not exhibit grey-body behaviour, it can be assumed that if the two wavelengths are carefully selected and are close enough to each other, the grey-body assumption is realistic [6, 18], but the measurement uncertainty also increases if the wavelengths get too close to each other [2, 20]), in which $\varepsilon_{s,1} = \varepsilon_{s,2} = \varepsilon_s$, surface temperature

$$T_s = \frac{c_2(\lambda_2 - \lambda_1)}{\lambda_1 \lambda_2 \left(\ln \frac{s_2 k_1}{s_1 k_2} + 5 \ln \frac{\lambda_2}{\lambda_1} \right)}, \tag{13}$$

and surface emissivity

$$\varepsilon_s = \frac{s_1 \lambda_1^5}{k_1 c_1} \exp \frac{c_2}{\lambda_1 T_s} = \frac{s_2 \lambda_2^5}{k_2 c_1} \exp \frac{c_2}{\lambda_2 T_s}. \tag{14}$$

Madura and Piątkowski [58] investigated a variation of the radiation ratio method, in which surface emissivity is assumed to be a power function of wavelength, so as to compensate for the non-grey effects of metallic surfaces, and concluded that measurement errors can be reduced for the changes introduced to the radiation ratio equation.

For partial and obstructed targets, equation (12) can be reformulated by replacing the fraction of visibility of the target surface by emissivities $\varepsilon_{s,1}$ and $\varepsilon_{s,2}$. As the fraction of visibility is the same for both wavelengths, the target temperature can be expressed by equation (13) [54]. However, the emissivity of the target surface must be known or constant for both spectral channels, and, in order to ensure that the effects of background radiation can be ignored, the obstruction must be cold relative to the target.

2.1.2. Temperature method. In the temperature method, equation (9) is simplified according to the aforementioned assumptions, resulting in the following system of two equations for the two spectral channels $i = 1$ and 2:

$$\varepsilon_{s,i} L_b(\lambda_i, T_s) = L_b(\lambda_i, T_i), \tag{15}$$

where T_i is the effective radiance temperature output, and $\varepsilon_{s,i} = \varepsilon_s(\lambda_i)$ is the emissivity of the target surface at wavelength λ_i. Solving equation (15) for T_s results in the so-called temperature ratio equation [57]:

$$\frac{1}{T_s} = \frac{1}{\lambda_2 - \lambda_1} \left(\frac{\lambda_2}{T_1} - \frac{\lambda_1}{T_2} + \frac{\lambda_1 \lambda_2}{c_2} \ln \frac{\varepsilon_{s,1}}{\varepsilon_{s,2}} \right). \tag{16}$$

For a grey target surface, in which $\varepsilon_{s,1} = \varepsilon_{s,2} = \varepsilon_s$, surface temperature

$$T_s = \frac{(\lambda_2 - \lambda_1) T_1 T_2}{\lambda_2 T_2 - \lambda_1 T_1}, \tag{17}$$

and surface emissivity

$$\varepsilon_s = \exp \left[\frac{c_2}{\lambda_1} \left(\frac{1}{T_s} - \frac{1}{T_1} \right) \right] = \exp \left[\frac{c_2}{\lambda_2} \left(\frac{1}{T_s} - \frac{1}{T_2} \right) \right]. \tag{18}$$

Tsai *et al* [57] investigated variations of the temperature ratio equation to compensate for the non-grey effects of real surfaces, conducted a series of experiments on aluminium alloys with different surface characteristics, concluding that dual-wavelength algorithms that account for different surface conditions result in improved accuracy, but prior knowledge of the target emissivity behaviour is required for the selection of the most appropriate algorithm.

For partial and obstructed targets, as for the radiation method, by replacing emissivities $\varepsilon_{s,1}$ and $\varepsilon_{s,2}$ by the fraction of target visibility in equation (16), the target temperature can be expressed by equation (17) [54].

2.2. Soot pyrometry

Basically, dual-wavelength soot pyrometry is a technique for the measurement of the temperature and/or concentration of soot present in combustion flames. Based on equation (9), assuming that background radiation effects are ignored, and all incoming radiation is absorbed at discrete wavelengths λ_i, for spectral channels $i = 1$ and 2,

$$\varepsilon_s(\lambda_i) L_b(\lambda_i, T_s) = L_b(\lambda_i, T_i), \tag{19}$$

where T_i is the is the effective radiance temperature output, T_s is the soot temperature, and $\varepsilon_s(\lambda_i)$ is the soot emissivity at wavelength λ_i. Although this expression is based on the temperature method discussed in section 2.1.2, an expression for the radiation method, as developed in section 2.1.1 for surface pyrometry, can also be used to model soot pyrometry [59]. Although black-body radiation emission is represented by Planck's spectral distribution (1), for low wavelengths and temperatures, Wien's spectral distribution (2) can also be applied to model black-body spectral radiation [60]. Generally, soot emissivity cannot be approximated to a grey surface, and according to the type of spectral function used to model soot emissivity, two distinct approaches have been developed to model dual-wavelength soot pyrometry [59–61]: the α-method and the F-method.

The α-method is based on the following relationship between soot emissivity and wavelength, as proposed by Hottel and Broughton [62, 63]:

$$\varepsilon_s(\lambda_i) = 1 - \exp \left(-\frac{\kappa l}{\lambda_i^{\alpha_i}} \right), \tag{20}$$

where κ is a factor proportional to soot concentration, l is the optical path length, and α_i is an empirical parameter. As product κl does not depend on temperature nor on emissivity, by simultaneously solving equations (19) and (20) for $i = 1$ and 2, through the elimination of κl, the following equation can be derived:

$$\left[1 - \frac{L_b(\lambda_1, T_s)}{L_b(\lambda_1, T_1)}\right]^{\lambda_1^{\alpha_1}} = \left[1 - \frac{L_b(\lambda_2, T_s)}{L_b(\lambda_2, T_2)}\right]^{\lambda_2^{\alpha_2}}. \quad (21)$$

If temperature outputs T_1 and T_2 are known for wavelengths λ_1 and λ_2, respectively, equation (21) can be solved for soot temperature T_s. Empirical parameter α_i is related to wavelength λ_i, particle size and refractive index of soot, and fuel type [64, 65]. Different α_i values were obtained by different researchers, for different wavelengths and fuel types, which can be found, for example, in the compilations performed by Zhao and Ladommatos [64] and Said *et al* [65]. However, if λ_i falls into the visible region, the choice of α_i is less critical, and a fixed value of $\alpha_i = 1.39$ is appropriate for most fuels [62–64].

In the F-method, emissivity is modelled according to Rayleigh's theory for small particles [63]:

$$\varepsilon_s(\lambda_i) = 1 - \exp\left(-36\pi \frac{F_i}{\lambda_i} f_v l\right), \quad (22)$$

where f_v is the soot volume fraction, l is the optical path length, $F_i = n_i k_i / [(n_i^2 - k_i^2 + 2)^2 + 4n_i^2 k_i^2]$, and n_i and k_i are the real and imaginary parts of the refraction index of soot, respectively, which are dependent on wavelength λ_i; for example, Chang and Charalampopoulos [66] modelled parameters n_i and k_i as cubic polynomials of $\ln \lambda_i$. As product $f_v l$ does not depend on temperature nor on emissivity, by simultaneously solving equations (19) and (22) for $i = 1$ and 2, through the elimination of $f_v l$, the following equation is obtained:

$$\left[1 - \frac{L_b(\lambda_1, T_s)}{L_b(\lambda_1, T_1)}\right]^{\lambda_1/F_1} = \left[1 - \frac{L_b(\lambda_2, T_s)}{L_b(\lambda_2, T_2)}\right]^{\lambda_2/F_2}. \quad (23)$$

As for equation (21), if temperatures T_1 and T_2 are known for wavelengths λ_1 and λ_2, equation (23) can be solved for temperature T_s.

Di Stasio and Massoli [60] presented a sensitivity analysis of the dual-wavelength pyrometry technique to calculate temperature T_s and volume fraction f_v, taking into account, for high and low soot concentration regimes, the influence of the following parameters: soot concentration, particle shape and size distribution, soot emissivity spectral functions α_i and F_i, and wavelengths λ_1 and λ_2. The authors concluded that the F-method always results in higher uncertainties when compared to the α-method; T_s and f_v are very sensitive to the soot refraction index but almost insensitive to the size distribution of soot particles; for wavelengths above 1.2 μm, uncertainties become very high, especially for low soot concentrations, indicating that visible wavelengths are more favourable for dual-wavelength soot temperature measurements. However, Jenkins and Hanson [59] argued that the radiation intensity in the visible range is lower than that in the IR range, resulting in low signal-to-noise ratios and, consequently, in high uncertainties in the visible range. Typical applications of dual-wavelength soot pyrometry systems include the measurement of soot temperature and/or volume fraction of diffusion and/or premix open flames [67–72] and also of pulverized coal flames [73–75]. However, as exposed throughout the next two paragraphs, most published works on dual-wavelength soot pyrometry are related to the combustion process in diesel engines.

Beatrice *et al* [61] investigated the volume fraction measurement of soot in diesel engines, concluding that the dual-wavelength method is appropriate to investigate the generation of particles during the combustion of different fuels. Zhao and Ladommatos [64] reviewed difference optical techniques to measure soot temperature and concentration in diesel engines, including the analysis of the most appropriate α_i values, the most favourable monochromatic wavelengths λ_1 and λ_2, and the examination of calibration procedures, concluding that $\alpha_i \approx 1$ is a reasonable fixed value for diesel soot in the IR range of 0.8–7 μm, visible wavelengths are preferred over IR wavelengths, and a large separation between λ_1 and λ_2 improves the sensitivity of dual-wavelength systems, provided that parameters α_1 and α_2 are accurately known. A recent work published by López *et al* [53] reported the implementation of the dual-wavelength method to evaluate factor κl of soot generated under real diesel engine conditions.

In diesel engine combustion, it is often desirable to obtain a two-dimensional distribution of temperature and/or concentration of soot. Dual-wavelength two-dimensional imaging techniques were reviewed by Zhao and Ladommatos [64]. Vattulainen *et al* [76] described a dual-wavelength imaging system, constructed with commercially available components, to perform soot temperature measurements in large diesel engines. Other examples of dual-wavelength imaging pyrometry on diesel engines include the influence of the propagation of calibration uncertainties on temperature T_s and factor κl [77], a computer model to investigate the spacial gradient effects of soot temperature and soot volume fraction on dual-wavelength pyrometry [78], and various studies that employ dual-wavelength imaging pyrometry to analyse diesel combustion processes [47, 49–52].

More advanced soot pyrometry systems, such as higher-order multi-wavelength and multi-band pyrometers, in which $n \geqslant 3$, have been published more recently [48, 79–82].

3. Multi-wavelength pyrometry

In theory, the limitation of dual-wavelength systems to grey surfaces can be overcome by increasing the number of measuring wavelengths, i.e. through higher-order multi-wavelength pyrometry systems, in which the number of simultaneous spectral measurements $n \geqslant 3$. Generally, surface emissivity is modelled as a function of wavelength and also of a set of m adjustable parameters, i.e. $a_0, a_1, \ldots, a_{m-1}$, where $n \geqslant m + 1$. In multi-wavelength pyrometry, it is assumed that the spectral bands are so narrow, i.e. $\lambda' \approx \lambda''$, that all incoming radiation is absorbed at discrete wavelengths λ_i for spectral measurements $i = 1, 2, \ldots, n$. According to equation (7), the output signal

of the pyrometers is proportional to the radiation absorbed by the detectors, so that, in a multi-wavelength system, if the effects of internal radiation are neglected, the following system of n equations and $m+1$ unknowns (m emissivity parameters $a_0, a_1, \ldots, a_{m-1}$ and surface temperature T_s) can be established:

$$s_i = k_i\{\varepsilon_s(\lambda_i)L_b(\lambda_i, T_s) + [1-\varepsilon_s(\lambda_i)]L_b(\lambda_i, T_a)\}, \tag{24}$$

where s_i is the output signal of spectral channel i, and k_i is a proportionality constant, obtainable from the calibration process, which depends on the electronic gain, system optics, and detector response at wavelength λ_i. Assuming Wien's distribution (2) to model black-body radiation and negligible background radiation effects, equation (24) reduces to the following system of equations:

$$\ln\frac{s_i\lambda_i^5}{k_i} = \ln\varepsilon_s(\lambda_i) - \frac{c_2}{\lambda_i T_s}. \tag{25}$$

Likewise, applying equation (9) to a multi-wavelength system results in the following system of n equations and $m+1$ unknowns (m emissivity parameters and temperature T_s):

$$\varepsilon_s(\lambda_i)L_b(\lambda_i, T_s) + [1-\varepsilon_s(\lambda_i)]L_b(\lambda_i, T_a) = L_b(\lambda_i, T_i), \tag{26}$$

where T_i is the effective radiance temperature output of spectral channel i. Assuming Wien's distribution (2) to model black-body radiation and negligible background radiation effects, equation (26) reduces to the following system of equations:

$$\frac{c_2}{\lambda_i T_i} = \frac{c_2}{\lambda_i T_s} - \ln\varepsilon_s(\lambda_i). \tag{27}$$

An essential condition for the successful application of multi-wavelength pyrometry systems is the choice of an adequate emissivity function. Two functions have been the most commonly used in emissivity modelling of multi-wavelength pyrometry systems [2, 83, 84]: the polynomial dependence of emissivity on wavelength,

$$\varepsilon_s(\lambda_i) = a_0 + a_1\lambda_i + \cdots + a_{m-1}\lambda_i^{m-1}, \tag{28}$$

and the polynomial dependence of the natural logarithm of emissivity on wavelength,

$$\ln\varepsilon_s(\lambda_i) = a_0 + a_1\lambda_i + \cdots + a_{m-1}\lambda_i^{m-1}. \tag{29}$$

Early works on multi-wavelength pyrometry produced controversial and rather divergent results, in which the output errors were reported to be relatively small in some cases but unacceptably high in other cases, depending on the material, state of the target surface, and the chosen emissivity function [2, 85].

Coates [86] applied equation (29) with $m = n-1$ parameters, i.e. $\ln\varepsilon_s(\lambda_i) = a_0 + a_1\lambda_i + \cdots + a_{n-2}\lambda_i^{n-2}$, into equation (25), resulting in a determined system of n equations with n unknowns ($n-1$ emissivity parameters and temperature T_s), whose solutions can be obtained by simple linear algebra. Afterwards, Coates derived an equation for the temperature error, expressed as the difference between predicted and true target temperatures. With n ranging from 1 to 10, it was concluded that, even in the absence of measurement errors, for $n \geqslant 4$, temperature errors become excessively large. The effect of measurement errors showed that only pyrometers with $n \leqslant 2$ are advantageous, since temperature errors increase extremely fast with increasing n. The growth of temperature errors with increasing n in determined systems was attributed to model over-fitting. It was suggested that over-fitting may be removed if $n \gtrsim 2m$, resulting in a overdetermined system to be solved by least-squares, but the author also concluded that prior knowledge of the dependence of spectral emissivity on wavelength is still necessary.

Basically, the least-squares method, applied to overdetermined multi-wavelength systems with n spectral measurements, is based on equation (24), through the minimization of the following error function:

$$\chi^2 = \sum_{i=1}^{n}(s_i - k_i\{\varepsilon_s(\lambda_i)L_b(\lambda_i, T_s) + [1-\varepsilon_s(\lambda_i)]L_b(\lambda_i, T_a)\})^2, \tag{30}$$

where s_i is the output signal, k_i is a proportionality constant, λ_i is the wavelength of spectral channel i, $\varepsilon_s(\lambda_i)$ is the emissivity at wavelength λ_i, T_s is the temperature of the target surface, and T_a is the temperature of the background surfaces. Emissivity parameters $a_0, a_1, \ldots, a_{m-1}$ and temperature T_s are the solutions to be evaluated by the least-squares method. The least-squares method may also be based on equation (26), through the minimization of the following error function:

$$\chi^2 = \sum_{i=1}^{n}(L_b(\lambda_i, T_i) - \{\varepsilon_s(\lambda_i)L_b(\lambda_i, T_s) + [1-\varepsilon_s(\lambda_i)]L_b(\lambda_i, T_a)\})^2, \tag{31}$$

where T_i is the temperature output of channel i.

Khan *et al* [20] analysed the ratio pyrometry technique for determined systems, in which the temperature is formulated independently of emissivity, with $n = 2$, 3, and 4 spectral channels. The ratio technique was used to simulate temperature measurements using multi-wavelength determined systems. It was concluded that there is no advantage in using the ratio technique for systems with $n > 2$, even in the absence of measurement noise, and the addition of noise to the input data considerably aggravates the uncertainty of temperature estimates. In a succeeding paper, Khan *et al* [21] analysed multi-wavelength overdetermined systems ($n > m+1$) using linear and non-linear least-squares. In linear least-squares, the emissivity function is restricted to the polynomial relationship between the natural logarithm of emissivity and wavelength (29), and black-body radiation is approximated to Wien's distribution (2). In non-linear least-squares, the emissivity function can be of any type, and Planck's distribution (1) can be used to model black-body radiation. A multi-wavelength pyrometry model was simulated to test the linear and non-linear least-squares techniques, indicating that the uncertainty of temperature predictions is closely related to the level of measurement noise and the validity of the selected emissivity function. The authors also developed a multi-wavelength pyrometer to measure the temperatures of various sources, reporting an accuracy of around 0.5%.

Saunders [87] presented a method for compensating for the effects of background radiation reflections in determined multi-wavelength systems, concluding that the uncertainties due to background radiation may be larger than the uncertainties encountered in single-wavelength pyrometry, so that the use of multi-wavelength pyrometers may even become impracticable.

If the effects of background and internal radiation are ignored, output signal s_i of a multi-wavelength pyrometer is expressed by equation (11), defined for $i = 1, 2, \ldots, n$ spectral channels. Using Wien's distribution (2) to model target radiation, equation (11) can be further expressed as follows (taking the natural logarithm of both sides and after algebraic manipulation):

$$\frac{1}{T_s} - \frac{\lambda_i}{c_2} \ln \varepsilon_{s,i} = \frac{\lambda_i}{c_2} \ln \frac{k_i c_1}{s_i \lambda_i^5}. \tag{32}$$

The calibration with a black body enables the quantification of proportionality constant k_i for every spectral channel i, so that the right-hand side of equation (32) becomes a known quantity, dependent on multi-wavelength output s_i, whereas the left-hand side of equation (32) remains unknown, since it depends on T_s and $\varepsilon_s(\lambda_i)$. The assumption of wavelength-independent emissivity, implicit in dual-wavelength pyrometry, can now be verified, since if the right-hand side of equation (32) is plotted against λ_i, and n is sufficiently high, according to the left-hand side of equation (32), this relationship should form a straight line for the range of λ_i values for which $\varepsilon_{s,i}$ is constant. Furthermore, temperature T_s can also be calculated, since the vertical intercept of the straight line, i.e. when $\lambda_i = 0$ μm, equals $1/T_s$. Using a spectrometer with more that 400 spectral measurements, Ng and Fralick [88] developed a multi-wavelength pyrometer and used a similar approach to determine temperature T_s for different surfaces and environments, including more sophisticated features, such as atmospheric attenuation and transparency of the target surface.

Cassidy and Choueiri [89] considered the two emissivity functions represented by equations (28) and (29) with $m = 2$, i.e. $\varepsilon_s(\lambda_i) = a_0 + a_1\lambda_i$ and $\ln \varepsilon_s(\lambda_i) = a_0 + a_1\lambda_i$, respectively, and compared the linear and non-linear least-squares methods for multi-wavelength systems, in which $n = 4$, 6, 8, and 10 spectral channels. The Monte Carlo technique was applied to simulate the impact of the propagation of input uncertainties on the uncertainty of the estimated temperature output, which was reported to decrease with increasing n, for both linear and non-linear methods, except for the highest input uncertainties, where the non-linear method resulted in higher output uncertainties.

Wen and co-workers examined different emissivity models, including equations (28) and (29) with $m = 2$, 3, and 4, by evaluating the error of temperature predictions of aluminium alloy surfaces [84, 90–92] and steel surfaces [83, 93] at 600–800 K, using multi-wavelength pyrometry over different spectral ranges between 2 and 4.8 μm. Both linear and non-linear least-squares techniques were used, depending on the type of emissivity model. Better predictions were achieved for narrower wavelength ranges and for the simplest emissivity models. Contradicting previous findings [21, 86, 89], increasing n above $m + 1$ did not enhance the measurement accuracy.

Many other multi-wavelength devices and/or processing techniques can be found in the literature: a model to estimate emissivity errors generated during multi-wavelength measurements was developed by Mazikowski and Chrzanowski [94], who concluded that the incorrect selection of the emissivity function and fluctuations of the temperature of the target surface are the largest sources of errors, errors caused by the reflection of background radiation on the target surface can be quite significant, depending on the difference between background and surface temperatures, but other sources of error, such as electronic noise, calibration inaccuracies, and analog-to-digital resolution, can be insignificant in well-designed pyrometers; Sun *et al* [95] and Xing and co-workers [96, 97] proposed a multi-wavelength algorithm, in which, for all wavelengths, a linear relationship between emissivity and true temperature is assumed, so that no specific relationship between emissivity and wavelength has to be selected, allowing the simultaneous calculation of true temperatures and spectral emissivities from the measurement of two consecutive temperatures; Madura *et al* [98] developed a triple-wavelength determined pyrometry system ($n = 3$ and $m = 2$) with measuring wavelengths of 1.6, 1.8, and 2 μm, especially suitable for the measurement of temperatures of metallic surfaces, in which the three effective radiance temperature outputs and the three possible ratio temperatures (17), estimated from the three dual-wavelength combinations, were used to select the most appropriate emissivity functions; Duvaut [85] developed a multi-wavelength pyrometer for temperature and spectral emissivity measurements of metallic surfaces, applied in the visible range of 0.45–0.7 μm and in the IR range of 2–7 μm, using different emissivity functions, recommending, for temperatures between 600 and 1200 K, systems in the IR rather than the visible range; Svet and Sergeev [99] announced a determined triple-wavelength pyrometer ($n = 3$ and $m = 2$), in which the logarithm of the emissivity is assumed to vary linearly with wavelength, reporting temperature measurement errors below 1%; in multi-wavelength pyrometers, since the distance between wavelengths must be low, in order to minimize emissivity variations, but not so low, in order to minimize the uncertainty of temperature estimates, Rodiet and co-workers [100, 101] proposed a method for the optimum selection of wavelengths, through the reduction of the uncertainty of temperature estimates of target surfaces with non-uniform emissivity, considering a multi-wavelength determined system with $n = 4$ spectral channels.

Fu and co-workers [102, 103] described a multi-wavelength method, named multi-colour pyrometry, which assumes that a polynomial emissivity function (28) with $m = 2$, i.e. $\varepsilon_s(\lambda_{i,j}) = a_{0,j} + a_{1,j}\lambda_{i,j}$, is adequate in a narrow spectral region of width $\Delta\lambda$, where wavelength $\lambda_{i,j}$ is between $\lambda_j - \Delta\lambda/2$ and $\lambda_j + \Delta\lambda/2$. Therefore, as $m = 2$, the number of spectral measurements n per spectral band $j = 1, 2, \ldots, N$, where N is the number of spectral bands, must not be lower than $m + 1$, i.e. $n \geqslant 3$, resulting in a total of nN spectral measurements and, therefore, in a system of nN independent equations with $2N + 1$ unknowns ($2N$ emissivity parameters, $a_{0,j}$ and $a_{1,j}$, and temperature T_s) to be solved by non-linear least-squares:

$$\varepsilon_s(\lambda_{i,j})L_b(\lambda_{i,j}, T_s) + [1 - \varepsilon_s(\lambda_{i,j})]L_b(\lambda_{i,j}, T_a) = L_b(\lambda_{i,j}, T_{i,j}), \quad (33)$$

where $i = 1, 2, \ldots n$, $T_{i,j}$ is the effective radiance temperature output i in spectral band j, T_s and T_a are the temperatures of the target and background surfaces, respectively.

Fu *et al* [104] proposed a theoretical method to determine the temperature distribution of grey surfaces using a single-spot multi-wavelength pyrometer. Basically, the method is based on the fact that the spectral radiation intensity emitted by a non-isothermal surface is different from that emitted by an isothermal surface, being dependent on the specific temperature distribution. Therefore, if the target surface is divided into m different temperature ranges, for a pyrometer with $n > m + 1$ spectral channels, an overdetermined system of n equations and $m + 1$ unknowns (m temperature ranges and surface emissivity) can be establish, whose solution can be obtained by least-squares. Validation of the method was performed by simulating temperature measurements of a grey surface, divided into 31 temperature ranges, in which the temperature decreased linearly from 800 K in the centre to 500 K in the edge of the measuring spot, using a multi-wavelength pyrometer with 101 spectral channels in the range of 8–13 μm; the areas corresponding to the 31 temperature ranges were estimated with a maximum error of around 3%.

Other contributions from Fu and co-workers to the advances in multi-wavelength surface pyrometry include: the development of a fast-response multi-wavelength pyrometer for high-temperature measurements, up to around 1500 K, in which the emitted radiation is transmitted through flexible optical fibres, so as to operate in harsh environments, sensitive to the spectral range of 0.2–1.2 μm, using the aforementioned multi-colour pyrometry method [102]; application of the aforementioned multi-colour pyrometry method to process the temperature measurements of heating and cooling environments, in which the effects of the reflected background radiation are eliminated, using a multi-wavelength pyrometer with a spectral range of 1.1–2.4 μm, operating in the temperature range of 700–1700 K [103]; the application of a pulsed tunable laser to evaluate and correct the effects of spectral stray radiation (radiation scattered from the optical elements of the system and projected onto the detector) on the measurements of temperature using a multi-wavelength pyrometer, comprising 175 measuring wavelengths in the range of 1–1.65 μm, resulting in a significant improvement in the accuracy of the pyrometer [22]; the simulation of a multi-wavelength overdetermined pyrometry system to measure the temperature of a semi-transparent plate, in the temperature range of 600–700 K and IR wavelength range of 11–14 μm, using non-linear least-squares [105].

Hagqvist and co-workers [106, 107] proposed a multi-wavelength technique, based on radiation measurements performed with a spectrophotometer in the spectral range of 0.19–0.87 μm, for temperature measurements of target surfaces with varying emissivity and temperature. It was assumed that the emissivity can be estimated from the emissivity of a previous instant, the technique does not require any assumed emissivity function, but it requires that the variation of emissivity with time and temperature is smooth. It also requires that, at least, an accurate value of surface temperature or emissivity is known at some instant (a thermocouple was used for initial temperature estimates). A titanium alloy surface was tested for temperature measurements in the range of 900–1400 K, and an error lower than 4% was reported for temperature estimates.

Girard *et al* [108] investigated the possible advantages in extending the operating wavelengths of a multi-wavelength pyrometer toward the ultraviolet (UV) region. Multi-wavelength temperature measurements of a target surface at 2000 °C were simulated for two wavelength ranges: 0.65–0.95 μm and 0.35–0.95 μm. A noise level of 0.1% was added to the simulated output signals, and the pyrometry model was based on equation (25), using the polynomial dependence of the natural logarithm of emissivity on wavelength (29) with m ranging from 1 to 4, resulting in overdetermined systems to be solved by linear least-squares. For all emissivity models, it was concluded that there is no real advantage to increase the number of spectral channels over 64, because the decrease of the uncertainty of the temperature estimates becomes negligible. The error of the simulated temperature estimates were reduced when the spectral content of the pyrometer channels were shifted towards the UV range, i.e. using range of 0.35–0.95 μm in place of 0.65–0.95 μm, being the error reduction more pronounced as m increased. Furthermore, Battuello and Girard [109] developed a UV multi-wavelength pyrometer for high-temperature applications (above 1300 °C), operating in the spectral range of 0.35–0.95 μm. By inserting optical windows of unknown transmissivities between the pyrometer and the target, the pyrometer was used to measure the temperature of a black body at 1300 °C, resulting in temperature measurement errors under 1%. Vuelban *et al* [110] described various radiometric techniques for determining the emissivity and temperature of an object, including the UV multi-wavelength pyrometry approach for simultaneous temperature and emissivity measurements.

4. Multi-band pyrometry

In multi-band pyrometry, the spectral channels cannot be assumed to be monochromatic, since the wavelength range of the spectral channels is too wide. Therefore, equations (24) and (26) are no longer valid to model multi-band systems, since the integrals between lower and upper cut-off wavelengths in equations (7) and (9) have to be evaluated. By assuming that in equation (7) the detector response remains constant between lower and upper cut-off wavelengths, if the effects of internal radiation are ignored, the following system of n equations can be established:

$$s_i = k_i \int_{\lambda=\lambda_i'}^{\lambda_i''} \{\varepsilon_s(\lambda)L_b(\lambda, T_s) + [1 - \varepsilon_s(\lambda)]L_b(\lambda, T_a)\}\, d\lambda, \quad (34)$$

where s_i is the output signal, k_i is a proportionality constant, obtainable from the calibration process, that depends on the electronic gain, system optics, and detector absorptivity, λ_i' and

λ_i'' are the lower and upper cut-off wavelengths, respectively, for spectral channels $i = 1, 2, \ldots, n$, T_s is the temperature of the target surface, and T_a is the background temperature.

By assuming that in equation (9) the detector response remains constant between lower and upper cut-off wavelengths, the following system of n equations can be established:

$$\int_{\lambda=\lambda_i'}^{\lambda_i''} \{\varepsilon_s(\lambda) L_b(\lambda, T_s) + [1 - \varepsilon_s(\lambda)] L_b(\lambda, T_a)\}\, d\lambda = \int_{\lambda=\lambda_i'}^{\lambda_i''} L_b(\lambda, T_i)\, d\lambda, \quad (35)$$

where T_i is the effective radiance temperature output, and λ_i' and λ_i'' are the lower and upper cut-off wavelengths, respectively, for spectral channels $i = 1, 2, \ldots, n$.

If Planck's distribution (1) is used to model black-body radiation, since the integrals over finite interval λ_i'– λ_i'' have no analytical solution [6], the solutions for equations (34) and (35) have to be achieved numerically, e.g. using the secant root-finding algorithm, along with the adaptive Simpson's method for numerical integration [7–10].

One major difficulty in multi-band pyrometry is the choice of the emissivity function $\varepsilon_s(\lambda)$. Simplest multi-band systems assume that the emissivity of the target surface does not vary with wavelength (grey surface assumption). Moreover, as stated in section 1, in place of equations (34) or (35), empirical-based relationships between the output signal of the pyrometer and the true temperature measured during the calibration process, such as equation (10), may be applied. For example, Small *et al* [16] developed a fibre-optic dual-band IR pyrometer, in which λ_1'–$\lambda_1'' = 2$–6 μm and λ_2'–$\lambda_2'' = 2$–12 μm, for low temperature measurements. The following calibration function was implemented for the two spectral channels $i = 1$ and 2:

$$s_{b,i} = \exp\left(A_i + \frac{B_i}{T} + C_i T\right), \quad (36)$$

where parameters A_i, B_i, and C_i were obtained by curve-fitting using the values of black-body temperature T and corresponding output signals $s_{b,i}$. Assuming that the target surface is grey, once parameters A_i, B_i, and C_i are known, the following system of two equations can be used to compute surface temperature and/or emissivity:

$$s_i = \varepsilon_s \exp\left(A_i + \frac{B_i}{T_s} + C_i T_s\right) + (1 - \varepsilon_s) \exp\left(A_i + \frac{B_i}{T_a} + C_i T_a\right), \quad (37)$$

where s_i are the output signals of the pyrometer for bands $i = 1$ and 2, T_a is the background temperature, assumed to be known, and the two unknowns T_s and ε_s are the temperature and emissivity of the target surface, respectively, whose solutions can be obtained implicitly from equation (37).

A different approach was proposed by Inagaki and Ishii [111], who developed a triple-band IR pyrometer, operating in the range of 2–13 μm, to measure near-ambient temperatures of surfaces with unknown emissivity and unknown background temperature. The effective radiance temperatures of the three spectral channels $i = 1$, 2, and 3 were expressed as follows:

$$T_i^{\alpha_{s,i}} = k_i T_s^{\alpha_{s,i}} = \varepsilon_s T_s^{\alpha_{s,i}} + (1 - \varepsilon_s) T_a^{\alpha_{a,i}}, \quad (38)$$

where T_i is the effective radiance temperature, T_s and T_a are the temperatures of the target and background surfaces, respectively, and ε_s is the emissivity of the target surface, assumed uniform for all three channels. Exponents $\alpha_{s,i}$ and $\alpha_{a,i}$ were determined by integrating the product of Planck's distribution (1) and the transmissivity of the IR filters for each spectral channel i, and as the difference between T_s and T_a is small, it was assumed that $\alpha_{s,i} = \alpha_{a,i}$. Since the values of T_i, $\alpha_{s,i}$, and $\alpha_{a,i}$ are known for each channels, equation (38) represents a determined system of six equation and unknowns T_s, ε_s, T_a, and k_i, which can be solved numerically to estimate T_s, ε_s, and T_a.

A potential modelling approach to dual-band pyrometry is based on the ratio method, described for dual-wavelength pyrometers in section 2.1.1, and on polynomial calibration functions. If a dual-band pyrometer is calibrated with a black body, the two output signals ($s_{b,1}$ and $s_{b,2}$) from the black-body measurements of different temperatures T_s can be modelled as two polynomials of order p:

$$s_{b,i} = \alpha_{0,i} + \alpha_{1,i} T_s + \cdots + \alpha_{p,i} T_s^p, \quad (39)$$

whose coefficients $\alpha_{0,i}, \alpha_{1,i}, \ldots, \alpha_{p,i}$ are to be obtained by data fitting, and $i = 1$ and 2 spectral channels. Furthermore, the ratio of the two output signals (s_1 and s_2) from the measurement of a target surface, whose mean emissivities over spectral bands λ_1'–λ_1'' and λ_2'–λ_2'' are $\bar{\varepsilon}_{s,1}$ and $\bar{\varepsilon}_{s,2}$, respectively, is given by the following expression:

$$\frac{s_1}{s_2} = \frac{\bar{\varepsilon}_{s,1} s_{b,1}}{\bar{\varepsilon}_{s,2} s_{b,2}} = \frac{\bar{\varepsilon}_{s,1}(\alpha_{0,1} + \alpha_{1,1} T_s + \cdots + \alpha_{p,1} T_s^p)}{\bar{\varepsilon}_{s,2}(\alpha_{0,2} + \alpha_{1,2} T_s + \cdots + \alpha_{p,2} T_s^p)}. \quad (40)$$

If $\bar{\varepsilon}_{s,1} \neq \bar{\varepsilon}_{s,2}$ (non-grey surface), ratio $\bar{\varepsilon}_{s,1}/\bar{\varepsilon}_{s,2}$ may be obtained by calibrating the pyrometer with a sample of the target surface at known temperatures T_s, by considering that $\bar{\varepsilon}_{s,1}/\bar{\varepsilon}_{s,2}$ can be approximated to a polynomial of order q in variable T_s:

$$\frac{\bar{\varepsilon}_{s,1}}{\bar{\varepsilon}_{s,2}} = \frac{s_1 s_{b,2}}{s_2 s_{b,1}} = \beta_0 + \beta_1 T_s + \cdots + \beta_q T_s^q, \quad (41)$$

where $\beta_0, \beta_1, \ldots, \beta_p$ are to obtained by data fitting. Therefore, if parameters $\alpha_{0,1}, \alpha_{1,1}, \ldots, \alpha_{p,1}$, $\alpha_{0,2}, \alpha_{1,2}, \ldots, \alpha_{p,2}$, and $\beta_0, \beta_1, \ldots, \beta_q$ are known, by replacing the emissivity ratio of equation (40) for the polynomial on the right-hand side of equation (41), if the same target surface is measured with the same pyrometer, surface temperature T_s can be estimated implicitly from equation (40), through a numerical procedure, using pyrometer outputs s_1 and s_2. Hijazi *et al* [18] develop an IR dual-band pyrometer based on a similar principle, operating in ranges of 3.8–4.4 μm and 4.1–5 μm, including more complex features, such as compensation for the effects of internal radiation. Aluminium alloy targets having two different surface roughness levels were tested, it was demonstrated that neither of the two surfaces exhibited grey-body behaviour, and temperature measurements were obtained with an error of less than 2%.

Lü *et al* [112] proposed an improved dual-band IR radiation pyrometer to measure the temperature of grey surfaces at low temperatures, which considered the influence of the ambient temperature on the radiation reflected by the target surface and on the stray radiation in the measurement system. The authors developed a modelling technique, based on the ratio method (section 2.1.1), adapted to include the effects of variable ambient temperature in dual-band systems, i.e. considering the integration of Planck's distribution (1) over the spectral range of the two measurement channels. Experimental results of grey-body measurements confirmed that that the proposed method is highly accurate with varying ambient temperature.

Assuming that the target surface is grey, and the background temperature is unknown, resulting in $m = 3$ unknowns (target temperature T_s, background temperature T_a, and wavelength-independent emissivity ε_s), in order to guarantee that equation (34) forms at least a determined system of equations, the number of spectral bands must not be less than three, i.e. $n \geqslant 3$. Uman *et al* [113] developed a model for an overdetermined fibre-optic pyrometry system with $n = 4$ or 5 spectral bands, concluding that there is no significant advantage when $n > 4$. Pyrometry measurements were performed to grey surfaces with $\varepsilon_s = 0.71$ and 0.8, $T_s = 45$–75 °C, and $T_a \approx 26$ °C. The estimated maximum errors obtained for T_s and T_a were of the order of 1%, and for ε_s were of the order of 10%.

Gao *et al* [114] described a quad-band pyrometer for temperature measurements of a target surface inside a narrow enclosure in the range of 700–1200 K, in which the background radiation effects cannot be ignored. Through the calculation of the view factor between the target surface and the enclosure inner walls, so as to compute the background radiation, and a technique involving a genetic algorithm to solve the multi-band modelling equations, assuming that the emissivity is unknown and non-uniform for different spectral channels, the authors claimed to be able to estimate the temperature of the target surface with an error of less than 0.5%.

Araújo and co-workers [7, 8] applied the Monte Carlo technique to calculate the uncertainties of temperature and emissivity estimates of grey surfaces at ambient temperature (300 K), using determined dual-band pyrometry systems ($n = 2$ and $m = 1$). A large number of simulations were performed, including the variation of the following parameters: uncertainty of the two effective radiance temperatures, emissivity of the target surface, background temperature, and spectral characteristics of the bands (bandwidth, location of the bands, and distance between bands, resulting in 78 different band combinations between 2 and 40 μm). In terms of the spectral characteristics of the bands, the authors concluded that narrow bands, far apart from each other, and shifted towards lower wavelengths decrease the output uncertainties of dual-band estimates. It was also concluded that the output uncertainties increase very rapidly as the background and target temperatures approach, but the output uncertainties decrease, tending to a minimum value, as the background and target temperatures depart from each other, regardless of whether the background temperature is higher or lower than the target temperature. However, by incorporating the uncertainties associated with the background temperature, Araújo [10] concluded that, when the background temperature is lower than the target temperature, the output uncertainties of dual-band estimates are virtually not affected by the uncertainty of the background temperature, but, contradicting previous findings [7, 8], when the background temperature is higher than the target temperature, the output uncertainties increase significantly with increasing uncertainty of the background temperature, so that dual-band output uncertainties increase even when the difference between background and target temperatures increases.

Araújo [9] proposed a higher-order multi-band pyrometry system for the measurement of grey surfaces at 300 K, in which $2 \leqslant n \leqslant 6$ and $m = 1$, by selecting twelve spectral bands from the wavelength range of 2–60 μm. The solution for surface temperature and emissivity was obtained by least-squares, i.e. through the minimization of the following error function:

$$\chi^2 = \sum_{i=1}^{n} \left\{ \int_{\lambda=\lambda_i'}^{\lambda_i''} L_b(\lambda, T_i)\, \mathrm{d}\,\lambda - \left[\varepsilon_s \int_{\lambda=\lambda_i'}^{\lambda_i''} L_b(\lambda, T_s)\, \mathrm{d}\lambda + (1-\varepsilon_s) \int_{\lambda=\lambda_i'}^{\lambda_i''} L_b(\lambda, T_a)\, \mathrm{d}\lambda \right] \right\}^2, \tag{42}$$

where T_i is the effective radiance temperature output, λ_i' and λ_i'' are the lower and upper cut-off wavelengths, respectively, for spectral channels $i = 1, 2, \ldots, n$, T_a is the background temperature, assumed to be known, and T_s and ε_s are the temperature and emissivity of the target surface, respectively, to be obtained by the least-squares method (42). The Monte Carlo technique was applied to calculate the uncertainties of temperature estimates, resulting from the propagation of the uncertainties of the effective radiance temperatures of the n spectral channels. Maximum reduction in the uncertainty of temperature estimates was obtained when n increased from 2 to 3, and only a small reduction was obtained when n increased from 3 to 4, with a negligible reduction for $n > 4$. Maximum uncertainty reductions from dual-band to higher-order multi-band systems were of the order of 10%, but some multi-band arrangements resulted in an increase in the uncertainty, indicating the importance of choosing the most appropriate multi-band spectral arrangement in order to guarantee that uncertainty is reduced.

Fu *et al* [115] proposed a novel optimization procedure to analyse the characteristics of multi-band pyrometry, based on two criteria: maximization of the sensitivity of the output signals with temperature variation; minimization of the variation of the sensitivity of the output signals with temperature variation. In order to validate the optimization criteria, the authors proposed a determined triple-band pyrometry system ($n = 3$ and $m = 2$), in which the emissivity function is a linear two-parameter relationship, and the spectral response of the detector is a Gaussian function:

$$\alpha_{d,i}(\lambda) = k_i \exp\left[-4 \ln 2 \left(\frac{\lambda - \overline{\lambda}_i}{\Delta\lambda_i} \right)^2 \right], \tag{43}$$

where k_i is the maximum of the sensor response, $\overline{\lambda}_i$ is the mean wavelength, and $\Delta\lambda_i$ is the wavelength width at half maximum, for $i = 1$, 2, and 3 spectral channels. In order to evaluate how the bandwidth of spectral function $\alpha_{d,i}(\lambda)$, i.e. parameter $\Delta\lambda_i$, affects temperature measurements, simulations were performed for $T_s = 1400$–2000 K, $k_1 = k_2 = k_3 = 1$, $\overline{\lambda}_1 = 0.48$ μm, $\overline{\lambda}_2 = 0.58$ μm, and $\overline{\lambda}_3 = 0.68$ μm, and $\Delta\lambda_1 = \Delta\lambda_2 = \Delta\lambda_3 = 0.01$–$0.5$ μm, demonstrating that different bandwidths $\Delta\lambda_i$ have a significant effect on the performance of multi-band pyrometers, and multi-wavelength pyrometers with monochromatic spectral channels are necessary not the best multi-spectral systems for temperature measurement. Fu *et al* [116] plotted curves of constant temperature and curves of constant ratio of emissivity function parameters against two normalized output signals, through simulations with the preceding values of k_i and $\overline{\lambda}_i$, for $\Delta\lambda_1 = \Delta\lambda_2 = \Delta\lambda_3 = 0.7$ μm, and different temperatures ranges selected between 1500 and 9000 K, providing an effective way to compute target temperature and emissivity parameters from different pyrometer output signals.

Fu *et al* [117] defined the signal measurement range of a radiation detector as the ratio of the maximum detection signal intensity, restricted by saturation, to the minimum detection signal intensity, restricted by noise, and defined the conditions by which the output signals of a triple-band pyrometer should be satisfied with respect to the signal measurement range. Afterwards, using the aforementioned optimization procedure [115], the authors proposed a method to assess the interrelated measurement ranges of surface temperature and ratio of emissivity function parameters. Experimental results of black-body measurements with a triple-band two-dimensional imaging pyrometer showed to be in agreement with the theoretical estimation of the measurement ranges of surface temperature.

Using a commercial digital colour camera, in which three images are simultaneously captured in the spectral ranges of the red, green, and blue (RGB) colours, respectively, Fu *et al* [118] developed a two-dimensional triple-band pyrometer, using a two-parameter linear emissivity model. The signal at spectral channel i was modelled as follows:

$$s_i = k_i \int_{\lambda=\lambda'}^{\lambda''} \alpha_{d,i}(\lambda)\varepsilon_s(\lambda)L_b(\lambda, T_s)\,d\lambda, \qquad (44)$$

where $i = 1$ for red, $i = 2$ for green, and $i = 3$ for blue, k_i is a proportionality constant, and $\alpha_{d,i}(\lambda)$ is the spectral response of the detector, including the effects of the optical system and colour filters. The range of the camera was λ'–$\lambda'' = 0.38$–0.78 μm. For each spectral channel, k_i and $\alpha_{d,i}(\lambda)$ were determined through a calibration procedure using a monochromator. The performance of the two-dimensional triple-band pyrometer was experimentally evaluated through black-body experiments in the temperature range of 1300–1900 °C, resulting in temperature errors in the order of 1%. Furthermore, Fu and co-workers [119, 120] developed a two-dimensional triple-band pyrometer, based on a commercial RGB-type sensor array, for high-temperature measurements. Raj and Prabhu [121] proposed a two-dimensional dual-band pyrometer to measure the temperature (above 500 °C) and emissivity of grey target surfaces, based on RGB colour images, using two empirical relationships obtained by fitting black-body calibration data to cubic splines: a relationship between black-body temperature and ratio s_1/s_2, where s_1 and s_2 are the output signals (44) of the red and green channels, respectively, and a relationship between s_1 and black-body temperature.

5. Final remarks

Multi-spectral pyrometry systems can be classified into two major classes, regarding the width of the spectral channels: multi-wavelength systems, in which the spectral channels are monochromatic, i.e. the width of each spectral channel is reduced to a single wavelength; and multi-band systems, in which the spectral channels have finite wavelength widths. Both pyrometry classes have their advantages and disadvantages, depending on whether the priority is the accuracy of the measurement or the simplicity of the signal processing technique.

Generally, as emissivity is wavelength-dependent, the multi-wavelength approach results in an underdetermined system of equations, i.e. there is one more unknown (an independent emissivity value for each spectral channel and surface temperature, resulting in $n + 1$ unknowns) than equations (an equation per spectral channel, resulting in n equations). In order to reduce the number of unknowns, so that the system of equations can be solved, the relationship between emissivity and wavelength has to be expressed by a mathematical function, having a number of unknown parameters that cannot exceed $n - 1$. If the number of unknown parameters equals $n - 1$, the system is said to be determined, having a unique solution for every emissivity parameter and surface temperature; if the number of unknown parameters is lower than $n - 1$, it results in an overdetermined system of equations, whose solution for emissivity parameters and surface temperature has to be obtained by least-squares.

The simplest multi-wavelength pyrometry processing techniques assume that black-body radiation is modelled by Wien's distribution, the target surface is much hotter than the surrounding surfaces, so that background radiation can be ignored, the natural logarithm of the emissivity is a polynomial function of wavelength, and there are as many unknowns as equations, resulting in a determined system of linear equations, whose unique solution can be obtained by simple linear algebra. However, as the accuracy of the estimates from determined multi-wavelength systems decreases very rapidly with increasing number of channels, these systems are limited to two or three channels only. Many dual-wavelength systems have been described in the literature, but this technique is restricted to grey surfaces, or if the ratio between the emissivities for both spectral channels is known. By increasing the number of spectral channels, so that the number of emissivity parameters is lower than $n - 1$ (overdetermined system), if all other assumptions are maintained, the solution for temperature and emissivity parameters can be obtained by linear least-squares. For other emissivity functions and/or if black-body radiation is modelled by Planck's distribution,

a non-linear least-squares technique has to be used to solve the overdetermined system of equations.

The processing of multi-band systems is much more complex, since the integration of Planck's distribution has to be performed for each spectral band, producing highly non-linear equations, so that system solutions can only be computed by numerical techniques, regardless of whether the system is determined or overdetermined. As for multi-wavelength systems, the emissivity has to be expressed as a function of wavelength, also having a number of unknown parameters that cannot exceed $n-1$. In terms of the spectral characteristics of the measurement bands, narrow bands, far apart from each other and shifted towards lower wavelengths, seem to provide more accurate solutions. However, narrower spectral bands imply less absorbed radiation and, consequently, lower signal-to-noise ratios. The simplest multi-band approaches rely on the grey surface assumption and on semi-empirical functions resembling Planck's distribution. More complex multi-band models use highly sophisticated numerical techniques to compute the solutions for temperature and/or emissivity function parameters.

Despite the numerous multi-spectral models proposed in the literature, it seems that there is not yet a consensual and universally accepted modelling technique to be applied for all situations. This is mainly due to the large errors arising from an inappropriate selection of the emissivity function, which is strongly dependent on the material and condition of the target surface. Therefore, the accuracy of any pyrometry system always depends on some prior knowledge of the emissivity of the target surface. Moreover, besides the unknown target surface emissivity and its unknown dependence on wavelength, there are other sources of uncertainty, such as the effects of background radiation and fluctuations of the target temperature, making multi-spectral pyrometry a rather challenging problem.

ORCID

António Araújo https://orcid.org/0000-0002-2879-1225

References

[1] DeWitt D P and Incropera F P 1988 Physics of thermal radiation *Theory and Practice of Radiation Thermometry* ed D P DeWitt and G D Nutter (Hoboken, NJ: Wiley) pp 21–89

[2] Krapez J-C 2011 Radiative measurements of temperature *Thermal Measurements and Inverse Techniques* ed H R B Orlande *et al* (Boca Raton, FL: CRC Press) pp 185–230

[3] Chrzanowski K 2001 *Non-Contact Thermometry: Measurement Errors* (Warsaw: SPIE Polish Chapter)

[4] Rogalski A 2003 Infrared detectors: status and trends *Prog. Quantum Electron.* **27** 59–210

[5] Minkina W and Dudzik S 2009 *Infrared Thermography: Errors and Uncertainties* (Chichester: Wiley)

[6] Modest M F 2013 *Radiative Heat Transfer* 3rd edn (San Diego, CA: Academic)

[7] Araújo A, Silvano S and Martins N 2014 Monte Carlo uncertainty simulation of surface emissivity at ambient temperature obtained by dual spectral infrared radiometry *Infrared Phys. Technol.* **67** 131–7

[8] Araújo A and Martins N 2015 Monte Carlo simulations of ambient temperature uncertainty determined by dual-band pyrometry *Meas. Sci. Technol.* **26** 085016

[9] Araújo A 2016 Analysis of multi-band pyrometry for emissivity and temperature measurements of gray surfaces at ambient temperature *Infrared Phys. Technol.* **76** 365–74

[10] Araújo A 2016 Dual-band pyrometry for emissivity and temperature measurements of gray surfaces at ambient temperature: the effect of pyrometer and background temperature uncertainties *Measurement* **94** 316–25

[11] Sakuma F and Hattori S 1982 Establishing a practical temperature standard by using a narrow-band radiation thermometer with a silicon detector *Temperature: Its Measurement and Control in Science and Industry* ed J F Schooley (New York: American Institute of Physics) pp 421–7

[12] Hahn J W and Rhee C 1994 Interpolation equation for the calibration of infrared pyrometers *Metrologia* **31** 27–32

[13] Saunders P 1997 General interpolation equations for the calibration of radiation thermometers *Metrologia* **34** 201–10

[14] Saunders P and White D R 2003 Physical basis of interpolation equations for radiation thermometry *Metrologia* **40** 195–203

[15] Sakuma F and Kobayashi M 1996 Interpolation equations of scales of radiation thermometers *Proc. TEMPMEKO '96, 6th Int. Symp. on Temperature and Thermal Measurements in Industry and Science (Torino)* pp 305–10

[16] Small W, Celliers P M, Da Silva L B, Matthews D L and Soltz B A 1998 Two-color mid-infrared thermometer with a hollow glass optical fiber *Appl. Opt.* **37** 6677–83

[17] Meola C and Carlomagno G M 2004 Recent advances in the use of infrared thermography *Meas. Sci. Technol.* **15** R27–58

[18] Hijazi A, Sachidanandan S, Singh R and Madhavan V 2011 A calibrated dual-wavelength infrared thermometry approach with non-greybody compensation for machining temperature measurements *Meas. Sci. Technol.* **22** 025106

[19] Liang M, Sun B, Sun X, Xie J and Yu C 2017 Rules of emissivity sample choice in multi-wavelength pyrometry *Int. J. Thermophys.* **38** 35

[20] Khan M A, Allemand C and Eagar T W 1991 Noncontact temperature measurement. I. Interpolation based techniques *Rev. Sci. Instrum.* **62** 392–402

[21] Khan M A, Allemand C and Eagar T W 1991 Noncontact temperature measurement. II. Least square based techniques *Rev. Sci. Instrum.* **62** 403–9

[22] Fu T, Duan M, Liu J and Li T 2014 Spectral stray light effect on high-temperature measurements using a near-infrared multi-wavelength pyrometer *Infrared Phys. Technol.* **67** 590–5

[23] Scaccabarozzi D, Saggin B, Baruffaldi D and Tarabini M 2016 Infrared thermometers for small wires drawing *Measurement* **80** 108–14

[24] Hunter G B, Allemand C D and Eagar T W 1985 Multiwavelength pyrometry: an improved method *Opt. Eng.* **24** 1081–5

[25] Duvaut Th, Georgeault D and Beaudoina J L 1996 Pyrométrie multispectrale infrarouge: application aux métaux *Rev. Gen. Therm.* **35** 185–96

[26] Yamazaki K, Yamamoto E, Suzuki K, Koshiishi F, Tashiro S, Tanaka M and Nakata K 2010 Measurement of surface temperature of weld pools by infrared two colour pyrometry *Sci. Technol. Weld. Joining* **15** 40–7

[27] Yamazaki K, Yamamoto E, Suzuki K, Koshiishi F, Waki K, Tashiro S, Tanaka M and Nakata K 2010 The measurement

of metal droplet temperature in GMA welding by infrared two-colour pyrometry *Weld. Int.* **24** 81–7
[28] Liang F, Tanaka M, Choi S and Watanabe T 2016 Investigation of the relationship between arc-anode attachment mode and anode temperature for nickel nanoparticle production by a DC arc discharge *J. Phys. D: Appl. Phys.* **49** 125201
[29] Meriaudeau F 2007 Real time multispectral high temperature measurement: application to control in the industry *Image Vis. Comput.* **25** 1124–33
[30] Hagqvist P, Kristoffersen H and Christiansson A-K 2014 Temperature monitoring of induction hardening using spectral pyrometry *Proc. 6th Int. Swedish Production Symp. (Gothenburg)*
[31] Ueda T, Sato M and Nakayama K 1998 The temperature of a single crystal diamond tool in turning *CIRP Ann.—Manuf. Technol.* **47** 41–4
[32] Ueda T, Hosokawa A, Oda K and Yamada K 2001 Temperature on flank face of cutting tool in high speed milling *CIRP Ann.—Manuf. Technol.* **50** 37–40
[33] Davies M A, Ueda T, M'Saoubi R, Mullany B and Cooke A L 2007 On the measurement of temperature in material removal processes *CIRP Ann.—Manuf. Technol.* **56** 581–604
[34] Ueda T, Sato M, Hosokawa A and Ozawa M 2008 Development of infrared radiation pyrometer with optical fibers—Two-color pyrometer with non-contact fiber coupler *CIRP Ann.—Manuf. Technol.* **57** 69–72
[35] Tapetado A, Diaz-Alvarez J, Miguelez M H and Vazquez C 2016 Two-color pyrometer for process temperature measurement during machining *J. Lightwave Technol.* **34** 1380–6
[36] Dagel D J, Grossetete G D, MacCallum D O and Korey S P 2016 Four-color imaging pyrometer for mapping temperatures of laser-based metal processes *Proc. SPIE* **9861** 986103
[37] Devesse W, De Baere D and Guillaume P 2017 High resolution temperature measurement of liquid stainless steel using hyperspectral imaging *Sensors* **17** 91
[38] Thevenet J, Siroux M and Desmet B 2010 Measurements of brake disc surface temperature and emissivity by two-color pyrometry *Appl. Therm. Eng.* **30** 753–9
[39] Kasem H, Thevenet J, Boidin X, Siroux M, Dufrenoy P, Desmet B and Desplanques Y 2010 An emissivity-corrected method for the accurate radiometric measurement of transient surface temperatures during braking *Tribol. Int.* **43** 1823–30
[40] Kasem H, Brunel J-F, Dufrenoy P, Desplanques Y and Desmet B 2012 Monitoring of temperature and emissivity during successive disc revolutions in braking *Proc. Inst. Mech. Eng. J: J. Eng. Tribol.* 226 748–59
[41] Estevadeordal J, Tralshawala N and Badami V 2013 Multi-color imaging pyrometry techniques for gas turbine engine applications *ASME 2013 Fluids Engineering Division Summer Meeting (Incline Village)* p V002T11A007
[42] Gao S, Wang L and Feng C 2014 Multi-spectral pyrometer for gas turbine blade temperature measurement *Proc. SPIE* **9202** 920217
[43] Ketui D, Chi F and Shan G 2016 Single wavelength and ratio pyrometry reflection errors in temperature measurement of gas turbine blade *Measurement* **86** 133–40
[44] Gao S, Feng C, Wang L and Li D 2016 Multi-spectral temperature measurement method for gas turbine blade *Opt. Rev.* **23** 17–25
[45] Daniel K, Feng C and Gao S 2016 Application of multispectral radiation thermometry in temperature measurement of thermal barrier coated surfaces *Measurement* **92** 218–23
[46] Madura H, Piątkowski T and Powiada E 2004 Multispectral precise pyrometer for measurement of seawater surface temperature *Infrared Phys. Technol.* **46** 69–73
[47] Han Y, Lee K and Min K 2009 A study on the measurement of temperature and soot in a constant-volume chamber and a visualized diesel engine using the two-color method *J. Mech. Sci. Technol.* **23** 3114–23
[48] Fu T, Wang Z and Cheng X 2010 Temperature measurements of diesel fuel combustion with multicolor pyrometry *J. Heat Transfer* **132** 051602
[49] Lee J, Oh H and Bae C 2012 Combustion process of JP-8 and fossil Diesel fuel in a heavy duty diesel engine using two-color thermometry *Fuel* **102** 264–73
[50] Zhang J, Jing W, Roberts W L and Fang T 2013 Soot temperature and KL factor for biodiesel and diesel spray combustion in a constant volume combustion chamber *Appl. Energy* **107** 52–65
[51] Zhang J, Jing W, Roberts W L and Fang T 2014 Soot measurements for diesel and biodiesel spray combustion under high temperature highly diluted ambient conditions *Fuel* **135** 340–51
[52] Jing W, Wu Z, Zhang W and Fang T 2015 Measurements of soot temperature and KL factor for spray combustion of biomass derived renewable fuels *Energy* **91** 758–71
[53] López J J, Martín J, García A, Villalta D and Warey A 2017 Implementation of two color method to investigate late cycle soot oxidation process in a CI engine under low load conditions *Appl. Therm. Eng.* **113** 878–90
[54] Tenney A S 1988 Radiation ratio thermometry *Theory and Practice of Radiation Thermometry* ed D P DeWitt and G D Nutter (Hoboken, NJ: Wiley) pp 459–94
[55] Love T J 1988 Environmental effects on radiation thermometry *Theory and Practice of Radiation Thermometry* ed D P DeWitt and G D Nutter (Hoboken, NJ: Wiley) pp 189–229
[56] Nutter G D 1988 Radiation thermometer: design principles and operating characteristics *Theory and Practice of Radiation Thermometry* ed D P DeWitt and G D Nutter (Hoboken, NJ: Wiley) pp 231–7
[57] Tsai B K, Shoemaker R L, DeWitt D P, Cowans B A, Dardas Z, Delgass W N and Dail G J 1990 Dual-wavelength radiation thermometry: emissivity compensation algorithms *Int. J. Thermophys.* **11** 269–81
[58] Madura H and Piątkowski T 2004 Emissivity compensation algorithms in double-band pyrometry *Infrared Phys. Technol.* **46** 185–9
[59] Jenkins T P and Hanson R K 2001 Soot pyrometry using modulated absorption/emission *Combust. Flame* **126** 1669–79
[60] di Stasio S and Massoli P 1994 Influence of the soot property uncertainties in temperature and volume-fraction measurements by two-colour pyrometry *Meas. Sci. Technol.* **5** 1453–65
[61] Beatrice C, Bertoli C, Cirillo N C, del Giacomo N and di Stasio S 1995 Two-colour pyrometry measurements of soot loading in a diesel engine burning model fuels of varying quality *Combust. Sci. Technol.* **110** 321–39
[62] Hottel H C and Broughton F P 1932 Determination of true temperature and total radiation from luminous gas flames *Ind. Eng. Chem.* **4** 166–74
[63] Howell J R and Siegel R 1971 Thermal radiation heat transfer: radiation transfer with absorbing, emitting, and scattering media *Technical Report* NASA Lewis Research Center Cleveland
[64] Zhao H and Ladommatos N 1998 Optical diagnostics for soot and temperature measurement in diesel engines *Prog. Energy. Combust. Sci.* **24** 221–55
[65] Said M A, Buttsworth D R and Yusaf T F 2009 A review of radiation heat transfer measurement for diesel engines using the two-colour method *Proc. 3rd International Conf. on Energy and Environment: Advancement Towards Global Sustainability (Mallaca)* pp 202–7

[66] Chang H and Charalampopoulos T T 1990 Determination of the wavelength dependence of refractive indices of flame soot *Proc. R. Soc. Lond.* A **430** 577–91
[67] Lee W and Na Y D 2000 Soot study in laminar diffusion flames at elevated pressure using two-color pyrometry and Abel inversion *JSME Int. J. Ser. B: Fluids Therm. Eng.* **43** 550–5
[68] Huang Y and Yan Y 2000 Transient two-dimensional temperature measurement of open flames by dual-spectral image analysis *Trans. Inst. Meas. Control* **22** 371–84
[69] Kuhn P B, Ma B, Connelly B C, Smooke M D and Long M B 2011 Soot and thin-filament pyrometry using a color digital camera *Proc. Combust. Inst.* **33** 743–50
[70] Zhang Z, Sun W, Shi L and Xing J 2012 Multi-wavelength pyrometry for temperature measurement in gas flames *Proc. Int. Conf. on Measurement, Information and Control (Harbin)* vol 1 pp 198–201
[71] Guo H, Castillo J A and Sunderland P B 2013 Digital camera measurements of soot temperature and soot volume fraction in axisymmetric flames *Appl. Opt.* **52** 8040–7
[72] Zhou Z, Tian D, Wu Z, Bian Z and Wu W 2015 3-D reconstruction of flame temperature distribution using tomographic and two-color pyrometric techniques *IEEE Trans. Instrum. Meas.* **64** 3075–84
[73] Levendis Y A, Estrada K R and Hottel H C 1992 Development of multicolor pyrometers to monitor the transient response of burning carbonaceous particles *Rev. Sci. Instrum.* **63** 3608–22
[74] Lu G, Yan Y, Riley G and Bheemul H C 2002 Concurrent measurement of temperature and soot concentration of pulverized coal flames *IEEE Trans. Instrum. Meas.* **51** 990–995
[75] Lu G, Yan Y, Cornwell S and Riley G 2005 Temperature profiling of pulverised coal flames using multi-colour pyrometric and digital imaging techniques *Proc. IEEE Instrumentation and Measurement Technology Conf. (Ottawa)* vol 3 pp 1658–62
[76] Vattulainen J, Nummela V, Hernberg R and Kytölä J 2000 A system for quantitative imaging diagnostics and its application to pyrometric in-cylinder flame-temperature measurements in large diesel engines *Meas. Sci. Technol.* **11** 103–19
[77] Payri F, Pastor J V, García J M and Pastor J M 2007 Contribution to the application of two-colour imaging to diesel combustion *Meas. Sci. Technol.* **18** 2579–98
[78] Musculus M P B, Singh S and Reitz R D 2008 Gradient effects on two-color soot optical pyrometry in a heavy-duty DI diesel engine *Combust. Flame* **153** 216–27
[79] Fu T, Cheng X and Yang Z 2008 Theoretical evaluation of measurement uncertainties of two-color pyrometry applied to optical diagnostics *Appl. Opt.* **47** 6112–23
[80] Khatami R and Levendis Y A 2011 On the deduction of single coal particle combustion temperature from three-color optical pyrometry *Combust. Flame* **158** 1822–36
[81] Ni M, Zhang H, Wang F, Xie Z, Huang Q, Yan J and Cen K 2016 Study on the detection of three-dimensional soot temperature and volume fraction fields of a laminar flame by multispectral imaging system *Appl. Therm. Eng.* **96** 421–31
[82] Yuan Y, Li S, Zhao F, Yao Q and Long M B 2016 Characterization on hetero-homogeneous ignition of pulverized coal particle streams using CH∗ chemiluminescence and 3 color pyrometry *Fuel* **184** 1000–6
[83] Wen C-D and Chr Y-H 2010 The assessment of multispectral radiation thermometry using linear and log-linear emissivity models for steel *Numer. Heat Transfer* B **58** 40–54
[84] Wen C-D and Chai T-Y 2011 Experimental investigation of emissivity of aluminum alloys and application of multispectral radiation thermometry *Appl. Therm. Eng.* **31** 2414–21
[85] Duvaut Th 2008 Comparison between multiwavelength infrared and visible pyrometry: application to metals *Infrared Phys. Technol.* **51** 292–9
[86] Coates P B 1981 Multi-wavelength pyrometry *Metrologia* **17** 103–9
[87] Saunders P 2000 Reflection errors and uncertainties for dual and multiwavelength pyrometers *High Temp.–High Press.* **32** 239–49
[88] Ng D and Fralick G 2001 Use of a multiwavelength pyrometer in several elevated temperature aerospace applications *Rev. Sci. Instrum.* **72** 1522–30
[89] Cassady L D and Choueiri E Y 2003 High accuracy multi-color pyrometry for high temperature surfaces *28th Int. Electric Propulsion Conf. (Toulouse)* pp 17–21
[90] Wen C-D and Mudawar I 2002 Experimental investigation of emissivity of aluminum alloys and temperature determination using multispectral radiation thermometry (MRT) algorithms *J. Mater. Eng. Perform.* **11** 551–62
[91] Wen C-D and Mudawar I 2005 Emissivity characteristics of polished aluminum alloy surfaces and assessment of multispectral radiation thermometry (MRT) emissivity models *Int. J. Heat Mass Transfer* **48** 1316–29
[92] Wen C-D 2011 Temperature determination using multispectral radiation thermometry algorithms for aluminum alloys *Heat Transfer Eng.* **32** 514–20
[93] Wen C-D 2010 Investigation of steel emissivity behaviors: examination of multispectral radiation thermometry (MRT) emissivity models *Int. J. Heat Mass Transfer* **53** 2035–43
[94] Mazikowski A and Chrzanowski K 2003 Non-contact multiband method for emissivity measurement *Infrared Phys. Technol.* **44** 91–9
[95] Sun X, Yuan G, Dai J and Chu Z 2005 Processing method of multi-wavelength pyrometer data for continuous temperature measurements *Int. J. Thermophys.* **26** 1255–61
[96] Xing J, Cui S, Qi W, Zhang F, Sun X and Sun W 2015 A data processing algorithm for multi-wavelength pyrometry which does not need to assume the emissivity model in advance *Measurement* **67** 92–8
[97] Xing J, Rana R S and Gu W 2016 Emissivity range constraints algorithm for multi-wavelength pyrometer (MWP) *Opt. Express* **24** 2955–7
[98] Madura H, Kastek M and Piątkowski T 2007 Automatic compensation of emissivity in three-wavelength pyrometers *Infrared Phys. Technol.* **51**
[99] Svet D Ya and Sergeev S S 2012 A triple-wavelength pyrometer that measures true temperature *Meas. Tech.* **54** 1–3
[100] Rodiet C, Remy B, Degiovanni A and Demeurie F 2013 Optimisation of wavelengths selection used for the multi-spectral temperature measurement by ordinary least squares method of surfaces exhibiting non-uniform emissivity *Quant. InfraRed Thermogr. J.* **10** 222–36
[101] Rodiet C, Remy B and Degiovanni A 2016 Optimal wavelengths obtained from laws analogous to the Wien's law for monospectral and bispectral methods, and general methodology for multispectral temperature measurements taking into account global transfer function including non-uniform emissivity of surfaces *Infrared Phys. Technol.* **76** 444–54
[102] Fu T, Tan P, Pang C, Zhao H and Shen Y 2011 Fast fiber-optic multi-wavelength pyrometer *Rev. Sci. Instrum.* **82** 064902
[103] Fu T, Liu J, Duan M and Zong A 2014 Temperature measurements using multicolor pyrometry in thermal radiation heating environments *Rev. Sci. Instrum.* **85** 044901

[104] Fu T, Duan M, Tian J and Shi C 2016 Inverse analysis of non-uniform temperature distributions using multispectral pyrometry *Infrared Phys. Technol.* **76** 504–9
[105] Fu T, Liu J, Tang J, Duan M, Zhao H and Shi C 2014 Temperature measurements of high-temperature semi-transparent infrared material using multi-wavelength pyrometry *Infrared Phys. Technol.* **66** 49–55
[106] Hagqvist P, Sikström F, Christiansson A-K and Lennartson B 2014 Emissivity compensated spectral pyrometry for varying emissivity metallic measurands *Meas. Sci. Technol.* **25** 025010
[107] Hagqvist P, Sikström F, Christiansson A-K and Lennartson B 2014 Emissivity compensated spectral pyrometry—algorithm and sensitivity analysis *Meas. Sci. Technol.* **25** 025011
[108] Girard F, Battuello M and Florio M 2014 Multiwavelength thermometry at high temperature: why it is advantageous to work in the ultraviolet *Int. J. Thermophys.* **35** 1401–13
[109] Battuello M and Girard F 2016 Characterisation and laboratory investigation of a new ultraviolet multi-wavelength measuring system for high-temperature applications *Measurement* **87** 126–37
[110] Vuelban E M, Girard F, Battuello M, Nemeček P, Maniur M, Pavlásek P and Paans T 2015 Radiometric techniques for emissivity and temperature measurements for industrial applications *Int. J. Thermophys.* **36** 1545–68
[111] Inagaki T and Ishii T 2000 On the proposal of quantitative temperature measurement by using three-color technique combined with several infrared sensors having different detection wavelength bands *Infrared Phys. Technol.* **41** 325–37
[112] Lü Y, He X, Wei Z-H, Sun Z-Y and Chang S-T 2016 Ambient temperature-independent dual-band mid-infrared radiation thermometry *Appl. Opt.* **55** 2169–74
[113] Uman I, Sade S, Gopal V, Harrington J A and Katzir A 2004 All-fiber-optic infrared multispectral radiometer for measurements of temperature and emissivity of graybodies at near-room temperature *Appl. Opt.* **43** 2039
[114] Gao S, Wang L, Feng C, Xiao Y and Daniel K 2015 Multi-spectral pyrometer for narrow space with high ambient temperature *Opt. Rev.* **22** 605–13
[115] Fu T, Cheng X, Fan X and Ding J 2004 The analysis of optimization criteria for multi-band pyrometry *Metrologia* **41** 305–13
[116] Fu T, Cheng X, Wu B, Zhong M, Shi C and Liu T 2006 The measurement coordinates for multi-band pyrometry *Meas. Sci. Technol.* **17** 379–83
[117] Fu T, Cheng X, Zhong M and Liu T 2006 The theoretical prediction analyses of the measurement range for multi-band pyrometry *Meas. Sci. Technol.* **17** 2751–6
[118] Fu T, Cheng X, Shi C, Zhong M, Liu T and Zheng X 2006 The set-up of a vision pyrometer *Meas. Sci. Technol.* **17** 659–65
[119] Fu T, Zhao H, Zeng J, Wang Z, Zhong M and Shi C 2010 Improvements to the three-color optical CCD-based pyrometer system *Appl. Opt.* **49** 5997–600
[120] Fu T, Yang Z, Wang L, Cheng X, Zhong M and Shi C 2010 Measurement performance of an optical CCD-based pyrometer system *Opt. Laser Technol.* **42** 586–93
[121] Raj V C and Prabhu S V 2013 Measurement of surface temperature and emissivity of different materials by two-colour pyrometry *Rev. Sci. Instrum.* **84** 124903